NANO LETTERS

Letter

pubs.acs.org/NanoLett

Sensing the Charge State of Single Gold Nanoparticles via Work Function Measurements

Yingjie Zhang,[†,‡] Olivier Pluchery,*[,§] Louis Caillard,[§,∥] Anne-Félicie Lamic-Humblot,[⊥] Sandra Casale,[⊥] Yves J. Chabal,[∥] and Miquel Salmeron*[,‡,#]

[†]Applied Science and Technology Graduate Program, University of California at Berkeley, Berkeley, California 94720, United States

[‡]Materials Sciences Division, Lawrence Berkeley National Laboratory, Berkeley, California 94720, United States

[§]UPMC Univ Paris 06, UMR CNRS 7588, Institut des NanoSciences de Paris, Sorbonne Universités, 4 place Jussieu, 75005 Paris, France

[∥]Laboratory for Surface and Nanostructure Modification, Department of Materials Science and Engineering, University of Texas at Dallas, 800 West Campbell Road, Dallas, Texas 75080, United States

[⊥]UPMC Univ Paris 06, UMR CNRS 7197, Laboratoire de Réactivité de Surface, Sorbonne Universités , 4 place Jussieu, 75005 Paris, France

[#]Department of Materials Science and Engineering, University of California at Berkeley, Berkeley, California 94720, United States

Supporting Information

ABSTRACT: Electrostatic interactions at the nanoscale can lead to novel properties and functionalities that bulk materials and devices do not have. Here we used Kelvin probe force microscopy (KPFM) to study the work function (WF) of gold nanoparticles (NPs) deposited on a Si wafer covered by a monolayer of alkyl chains, which provide a tunnel junction. We find that the WF of Au NPs is size-dependent and deviates strongly from that of the bulk Au. We attribute the WF change to the charging of the NPs, which is a consequence of the difference in WF between Au and the substrate. For an NP with 10 nm diameter charged with ~5 electrons, the WF is found to be only ~3.6 eV. A classical electrostatic model is derived that explains the observations in a quantitative way. We also demonstrate that the WF and charge state of Au NPs are influenced by chemical changes of the underlying substrate. Therefore, Au NPs could be used for chemical and biological sensing, whose environmentally sensitive charge state can be read out by work function measurements.

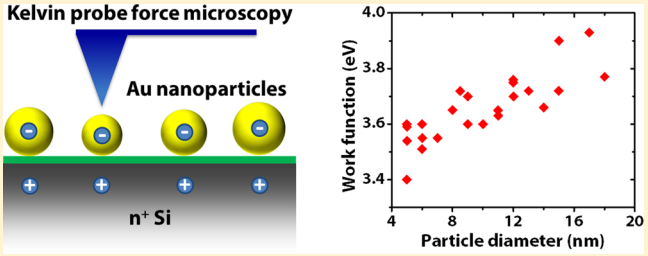

KEYWORDS: *Charge state, work function, gold nanoparticle, Kelvin probe force microscopy, chemical sensing*

When bulk materials are scaled down to the nanoscale, novel properties emerge, such as size-dependent bandgaps due to quantum confinement,[1,2] enhanced catalytic properties due to the large surface area and rich surface structure,[3,4] and plasmonic effects due to localized collective electron oscillation.[5,6] Another property that is often overlooked is the electrostatic interactions that lead to changes in work function, which is defined as the minimum thermodynamic work needed to extract an electron from a material to a point in vacuum immediately outside the surface.[7] As an example, Au nanoparticles from 3 nm to tens of nanometers are metallic,[8,9] although their WF deviates from that of the bulk Au, due to electrostatic effects.[10,11] For isolated neutral metal NPs, this is due to image force and Coulomb interactions.[10] However, when these NPs are interacting with the nearby environment, as is inevitable in device applications, their WF diverges from that of free particles.[12] In this case, the WF is no longer an intrinsic property of the NPs but depends critically on the chemical composition and electronic properties of the adjacent materials. Although electrostatic charge transfer was assumed to be responsible for the environmental dependence of the WF of metal NPs,[12] there has been no evidence or explanation of this effect. Here we report measurements of the change in the WF of Au NPs as a function of their size and explain the nature of the phenomenon by deriving a quantitative expression of the charge transfer. In contrast to atomic and molecular adsorbate systems that modify the WF of the substrate by the formation of electric dipole moments,[13,14] metal NPs exhibit unique nanoscale Coulomb confinement effects determining their WF.

Au NPs were deposited on a heavily n-doped silicon substrate precovered with an insulating monolayer film of alkyl chain molecules that provide a tunnel junction coupling between the NPs and the substrate. We expect that electrons will transfer from the Si to Au (due to their WF difference) by

Received: July 11, 2014
Revised: December 4, 2014
Published: December 8, 2014

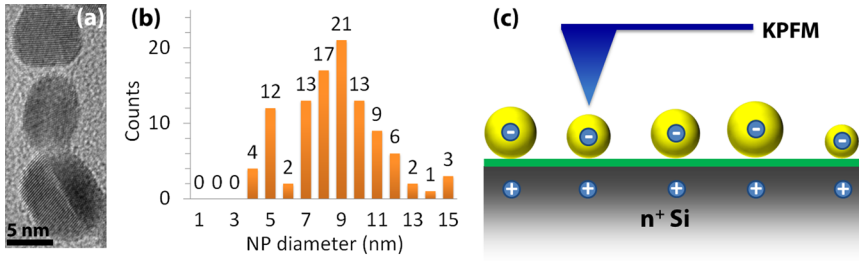

Figure 1. Au nanoparticles and work function measurements. (a) High-resolution TEM image showing three Au NPs. (b) Size distribution histogram analyzed from TEM images of 103 particles. (c) Schematic diagram of the KPFM measurements of the Au NPs deposited on a Si substrate covered with a grafted organic monolayer (GOM).

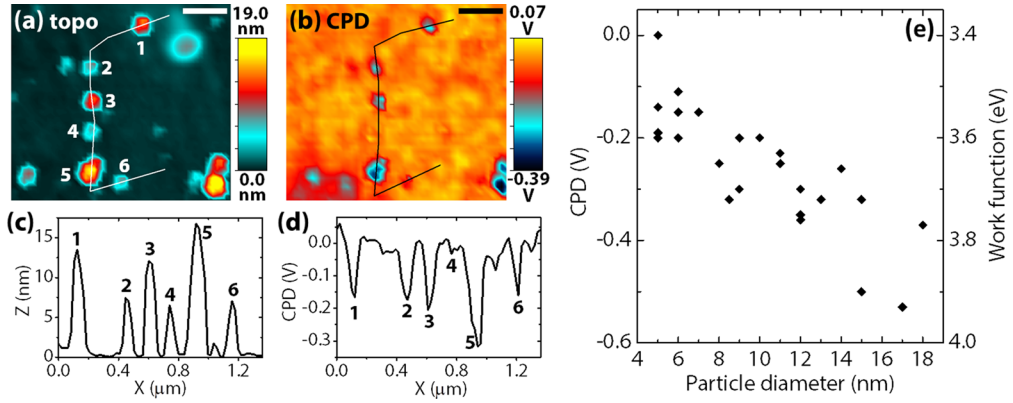

Figure 2. Nanoparticle work function versus size. (a,b) Simultaneously obtained topography and CPD images of NPs on the GOM covered Si substrate. Six NPs are labeled 1 to 6. Scale bar: 200 nm. The cross section profiles of topography (c) and CPD (d) indicate that in general the CPD is more negative when the NP size is larger. (e) CPD as a function of NP diameter (left scale). The right scale is the corresponding WF calibrated with the value determined by UPS on the GOM covered Si surface.

tunneling through the junction. The chemical inertness of Au and the ability to controllably oxidize the Si substrate make our sample an ideal platform to observe the effect of environmental factors on the charge state of Au NPs, and the consequent effect on WF change.

The gold nanoparticles were synthesized by reduction of a gold salt with ascorbic acid (see Supporting Information). Figure 1a shows transmission electron microscopy (TEM) images of three representative Au NPs. The NPs have a size distribution ranging from 3 to ~25 nm (Figure 1b) and are roughly spherical in shape. They were deposited on an amine-terminated C7 alkane monolayer grafted on heavily n-doped oxide-free Si(111) (phosphorus doped, 2×10^{18} cm^{-3}).[15,16] The amine group provides binding to the Au NPs. This grafted organic monolayer will be referred to as GOM. The ascorbic surfactants capping the NPs were removed prior to KPFM measurements with a 30 min annealing in vacuum at 150 °C. The GOM layer remained intact after this annealing process.[16] The GOM surface was not modified after annealing and the NP surface coverage remained ~1×10^9 cm^{-2} (10 NP/μm^2) as evaluated with atomic force microscopy (AFM).

The schematic setup of the KPFM measurement is shown in Figure 1c. The home-built single pass, frequency modulation KPFM has a resolution of ~10 mV.[17] During KPFM measurements, the sample was grounded, while a bias $V_{DC} + V_{AC} \cos\omega t$ was applied to the conductive AFM tip with $V_{AC} = 2$ V and $\omega = 2$ kHz. The electric field between the tip and surface, due to the contact potential difference and applied voltage, shifts the frequency and phase of the oscillating cantilever away from its free resonant value ($\omega_0 \approx 75$ *kHz*). It can be shown that the cantilever phase shift at ω is[18]

$$\Delta f_\omega \propto \frac{\partial^2 C}{\partial z^2}(V_{DC} - CPD_{tip-sample})V_{AC} \quad (1)$$

where $CPD_{tip-sample}$ is the contact potential difference between the tip and the sample. C is the tip−sample capacitance, and z is the tip−sample distance (typically <5 nm during imaging). V_{DC} is adjusted by the feedback control to maintain $\Delta f_\omega = 0$, so that its value is equal to the tip−sample contact potential difference. This compensation of the CPD also minimizes tip−sample electrostatic forces, allowing determination of the true sample topography.[18−21] For simplicity, in all the results shown here the CPD was calibrated by setting the average CPD of the GOM to zero. The calibrated CPD signal of the NP is related with its work function via the following relation:

$$\mathrm{CPD(NP)} = \frac{(W_{GOM} - W_{NP})}{e} \quad (2)$$

where W_{GOM} and W_{NP} are the work functions of the GOM and the Au NPs, respectively. e is the absolute value of the elementary charge. This relation shows that the changes in CPD and work function are of opposite sign.

With our setup, we obtain the surface topography and CPD images simultaneously in noncontact mode, allowing for a direct determination of NP size and WF. In contrast to electrostatic force microscopy, which can be utilized to manipulate the amount of charge in a tunnel junction,[22] KPFM can detect the WF of the NPs without changing their

dx.doi.org/10.1021/nl503782s | *Nano Lett.* 2015, 15, 51−55

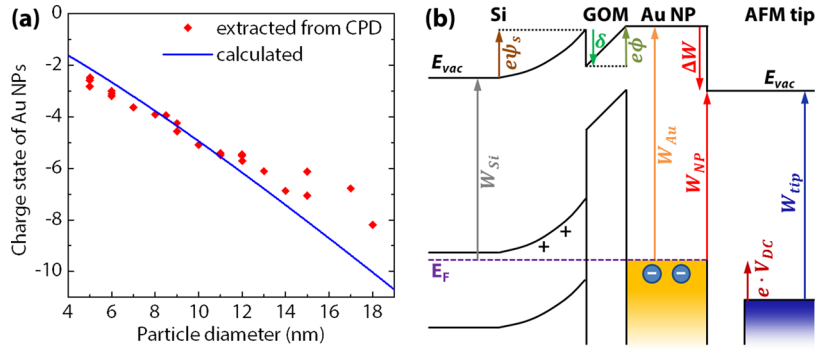

Figure 3. Charge state sensing and its mechanism. (a) Charge state of the Au NPs as extracted from the measured CPD and from calculations based on band diagram and capacitance analysis. (b) Band alignment diagram of the Au NP-GOM-Si junctions. The WF difference between charged Au NP and bulk Au (ΔW) arises mainly due to the Coulomb field produced by the charges inside the NP. The KPFM tip senses the WF of the NPs by applying a DC tip bias (V_{DC}) to align their vacuum level with that of the tip (eq 1). E_F, Fermi level; E_{vac}, vacuum level. ψ_s: band bending inside Si.

charge state, because the CPD is balanced by the tip bias to nullify the electric field.

Figure 2a,b shows topography and CPD images of one area. The height profile through 6 NPs shows a variation between 6 and 17 nm, which is in agreement with the NP size distribution measured by TEM. In the CPD image, the NPs appear as depressions (negative CPD), revealing that their WF is higher than that of the GOM on the Si(111) substrate. The GOM layer is electrically homogeneous, with a CPD fluctuation of less than 40 mV over the scanned area. As we can see in the profiles c and d, particle #5 has a size of 17 nm and a CPD of −310 mV, and particle #6 with a size of 7 nm has a CPD of −160 mV. Except for particle #4, the larger the NP, the more negative its CPD. A systematic study was carried out on 27 different NPs with sizes varying from 5 to 18 nm. A plot of the CPD (left scale) as a function of NP diameter (Figure 2e) shows that the CPD increases (i.e., WF decreases) when the NP diameter decreases. The work function of the GOM, found to be 3.4 eV by ultraviolet photoelectron spectroscopy (UPS), was used to obtain the WF of Au NPs (eq 2), as shown in the right scale in Figure 2e. We can see that the WF of Au NPs deviates substantially from that of the bulk Au ($W_{Au} \approx 5.1$ eV).[23] We note that our KPFM setup can only accurately measure the WF of NPs larger than 5 nm due to the limited spatial resolution imposed by our tip radius and imaging distance (Supporting Information). For this reason, the values for NPs smaller than 5 nm are not included. The data points for NPs larger than 20 nm are not included either due to their irregular shape. The observed 0.1−0.2 eV WF fluctuation of NPs with the same size can be due to the variation in particle shape and the orientation of the exposed facets[24] as well as from the presence of steps and kinks.[25]

Our results can be explained by the charge transferred between the substrate and the Au NP as a result of the mismatch between their work functions. The value of this charge is determined by the capacitance between the NP and the substrate. The charge produces an electrostatic field that leads to a change in the WF of the NPs. If instead of the NPs we had a metal film over the GOM, the Coulomb field would be zero above it (the field is confined between the film and the substrate). However, in the case of isolated nanoparticles the field extends outside with a value that depends on its size.

To calculate the Coulomb potential and to extract the charge state we start with Wood's formula[10] for neutral isolated metal nanospheres and modify it to derive the WF change of grounded charged metal nanospheres. The WF difference between a metal NP and the corresponding bulk metal (ΔW) arises from a difference in image force fields (ΔW_{im}) and from the Coulomb field near the surface of the NP due to the stored charges inside (ΔW_c)

$$\Delta W = \Delta W_{im} + \Delta W_C \tag{3}$$

The first term is the difference between the image potential energy at the surface of a sphere and that of a flat metal plane (Supporting Information)

$$\Delta W_{im} = -\frac{1}{8}\frac{1}{4\pi\varepsilon_0}\frac{e^2}{R} \tag{4}$$

where ε_0 is the vacuum permittivity, and R is the radius of the sphere. The charges inside the metal nanosphere, considered to reside at its center,[26] induce a Coulomb potential energy at the surface

$$\Delta W_C = N\frac{1}{4\pi\varepsilon_0}\frac{e^2}{R} \tag{5}$$

where N is the charge state of the NP, which can be either positive or negative. As we discuss in the Supporting Information, the contribution to N of the image charges from the depletion region in the Si substrate is negligible. Combining ΔW_{im} and ΔW_c we get

$$\Delta W = \left(2N - \frac{1}{4}\right)\frac{1}{4\pi\varepsilon_0}\frac{e^2}{D} \tag{6}$$

$$N = \frac{2\pi\varepsilon_0}{e^2}D\Delta W + \frac{1}{8} = \frac{D}{2.88\ \text{nm}\cdot\text{eV}}\Delta W + \frac{1}{8} \tag{7}$$

where D is the diameter of the sphere.

Using eq 7, we can extract the charge state of the Au NPs as a function of their diameter. The results are shown in Figure 3a. We can see that all the Au NPs are negatively charged, and the number of charges increases with the NP diameter.

To understand the mechanism of the charge storage we consider the band diagram shown in Figure 3b. The bulk work function of the n-doped Si is W_{Si} = 4.15 eV. There is a depletion region near the surface of the Si which contains positive charge as a result of electron transfer to the Au NP. In the region containing the GOM there is a potential energy drop of $\delta \approx -0.6$ eV due to the dipole moment at the Si-GOM interface and inside the GOM.[27−29] Since our NPs are larger

dx.doi.org/10.1021/nl503782s | Nano Lett. 2015, 15, 51−55

than 3 nm, their electronic properties are similar to those of bulk Au.[8,9] Therefore, the energy separation between vacuum level and Fermi level in the NP is nearly the same as that in bulk Au. Using a Poisson solver (Supporting Information), we calculated the built-in potential between the Au and the Si surface to be $\phi = 0.6\ V$.

To calculate the value of the charge in the Au NP (eN) for comparison with the measured results, we calculate the capacitance (C) of a gold sphere separated from a Si surface by a thin dielectric using a semianalytical formula (Supporting Information).[30] The charge state of the Au NPs was then calculated using $N = -\phi C/e$, shown in Figure 3a (blue line). The calculated values matches with those obtained from the CPD measurements. The small discrepancies for NPs larger than 15 nm may arise from the deviation of the NP shape from a sphere, as we have seen in TEM images (Supporting Information).

Because the charge state of metal NPs depends on the local electronic environment, their WF will also reflect local chemical changes. According to eq 6, the sensitivity of the WF on the charge state is 2.88 nm·eV/D per charge, which for a 5 nm NP amounts to ~0.6 eV. To demonstrate this effect we modified the surface chemistry of the Si substrate by oxidizing the sample by exposure to oxygen and measured the resulting change of WF of the Au NPs. We observed by X-ray photoelectron spectroscopy (XPS) and UPS that the Si(111) surface was fully oxidized after 3 days exposure to air, while the Au NPs remain intact. UPS also showed that the WF of the GOM-covered surface increased by 0.3 eV. With KPFM we imaged the CPD of the sample at different oxidation stages, and observed that the CPD of the GOM surface becomes inhomogeneous when partially oxidized (Figure 4a), and homogeneous again when the surface oxidation is complete (Figure 4b). The height distribution and shape of the Au NPs did not change with substrate oxidation.

We analyzed the WF and the extracted charge state of the fully oxidized sample as shown in Figure 4c,d. We observed an increase of WF for small NPs (5−15 nm), corresponding to a slight decrease in the amount of stored electrons. This can be explained by the decrease of capacitance between the Au NPs and the Si surface, as a result of the increased tunnel barrier thickness after Si surface oxidation (a quantitative calculation is shown in the Supporting Information). The WF is weakly dependent on the size of the NPs after substrate oxidation, while the charge state is more linearly dependent on the particle diameter (as shown by eq 7, a size-independent ΔW leads to $N \propto D$). This is a result of the linear dependence of C on NP size, which approaches the self-capacitance of the NP, as a result of the decreased coupling between the NP and substrate when the dielectric thickness increases. The change of the size-dependence of WF is more pronounced than that of the charge state, indicating that WF is very sensitive to changes of charge state. We therefore expect sensing applications where the chemical environment induces charge state changes of the metal NPs, which is amplified and detected by WF measurements.

In summary, we found that the work function of Au NPs is dominantly determined by their charge state and can deviate strongly from that of bulk Au. We can envision sensing applications based on this novel phenomenon, where scalable devices can be made using metal NPs, and the change of their WF can be detected via nanomechanical or capacitive measurements. Compared to the previously demonstrated single electron transistor devices[31] that require three terminals (source and drain need to be within tunneling range to the nano-island) and low-temperature operation, the WF-based charge sensing device only requires two terminals (source is within tunneling range to the NP, while sensing electrode can be a few nanometers away) and can operate at room temperature, opening up potential in situ chemical and biological sensing applications.

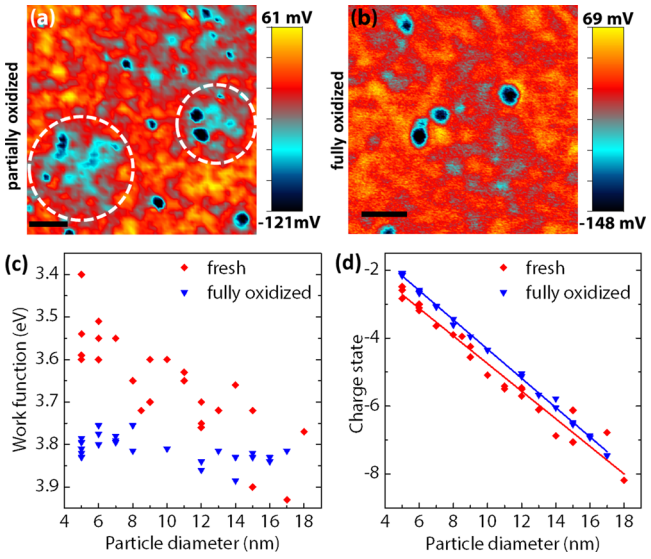

Figure 4. Effect of Si oxidation on the charge state and WF of the Au NPs. (a,b) CPD images of the sample after exposure in AFM chamber for 2 days (nitrogen purged, relative humidity below 0.5%) (a) and 3 days in air (b). Scale bar: 200 nm. In (a), the areas circled by white dashed lines and several other low CPD areas (blue/cyan areas) correspond to local oxidation spots. In (b) the surface is uniformly oxidized. (c) WF versus NP size for the fresh sample (same as Figure 2e) and for the fully oxidized sample (3 days exposure to air). (d) Charge state extracted from the WF in (c) with linear fits.

■ ASSOCIATED CONTENT

Supporting Information

Nanoparticle synthesis, GOM preparation, TEM imaging, stability of Au NPs during annealing, Kelvin probe force microscopy setup and resolution, discussions of the work function model, capacitance and potential calculations, CPD of Au NPs in different substrate oxidation stages, and charge state calculation of Au NPs on fully oxidized substrate. This material is available free of charge via the Internet at http://pubs.acs.org.

■ AUTHOR INFORMATION

Corresponding Authors

*E-mail: olivier.pluchery@insp.jussieu.fr (O.P.).
*E-mail: mbsalmeron@lbl.gov (M.S.).

Notes

The authors declare no competing financial interest.

■ ACKNOWLEDGMENTS

The KPFM part of this work was supported by NSF DMR-1104260, University of California, Davis and Berkeley. The sample preparation part was funded by the Grant CHE-1300180, University of Texas at Dallas. It used resources of the Molecular Foundry, a DOE Office of Science user facility. O.P. is grateful to his university (UPMC) for having granted him a sabbatical semester for initiating this work.

REFERENCES

(1) Talapin, D. V.; Lee, J.; Kovalenko, M. V.; Shevchenko, E. V. *Chem. Rev.* **2010**, *110*, 389−458.
(2) Li, L.; Hu, J.; Yang, W.; Alivisatos, A. P. *Nano Lett.* **2001**, *1*, 349−351.
(3) Bell, A. T. *Science* **2003**, *299*, 1688−1691.
(4) Cargnello, M.; Doan-Nguyen, V. V. T.; Gordon, T. R.; Diaz, R. E.; Stach, E. A.; Gorte, R. J.; Fornasiero, P.; Murray, C. B. *Science* **2013**, *341*, 771−773.
(5) Novotny, L.; van Hulst, N. *Nat. Photonics* **2011**, *5*, 83−90.
(6) Wang, H.; Brandl, D. W.; Le, F.; Nordlander, P.; Halas, N. J. *Nano Lett.* **2006**, *6*, 827−832.
(7) Kittel, C. *Introduction to Solid State Physics*, 7th ed.; Wiley: New York, 1995.
(8) Valdenm, M.; Lai, X.; Goodman, D. W. *Science* **1998**, *281*, 1647−1650.
(9) Häkkinen, H. Theoretical studies of gold nanoclusters in various chemical environments: when the size matters. In *Gold Nanoparticles for Physics, Chemistry and Biology*; Louis, C., Pluchery, O., Eds.; Imperal College Press: London, 2013.
(10) Wood, D. M. *Phys. Rev. Lett.* **1981**, *46*, 749.
(11) Zhou, L.; Zachariah, M. R. *Chem. Phys. Lett.* **2012**, *525−526*, 77−81.
(12) Stehlik, S.; Petit, T.; Girard, H. A.; Arnault, J.; Kromka, A.; Rezek, B. *Langmuir* **2013**, *29*, 1634−1641.
(13) Sasahara, A.; Pang, C. L.; Onishi, H. *J. Phys. Chem. B* **2006**, *110*, 17584−17588.
(14) de Boer, B.; Hadipour, A.; Mandoc, M. M.; van Woudenbergh, T.; Blom, P. W. M. *Adv. Mater.* **2005**, *17*, 621−625.
(15) Aureau, D.; Varin, Y.; Roodenko, K.; Seitz, O.; Pluchery, O.; Chabal, Y. J. *J. Phys. Chem. C* **2010**, *114*, 14180−14186.
(16) Caillard, L.; Seitz, O.; Campbell, P.; Doherty, R. P.; Lamic-Humblot, A.; Lacaze, E.; Chabel, Y. J.; Pluchery, O. *Langmuir* **2013**, *29*, 5066−5073.
(17) Zhang, Y.; Ziegler, D.; Salmeron, M. *ACS Nano* **2013**, *7*, 8258−8265.
(18) Li, G.; Mao, B.; Lan, F.; Liu, L. *Rev. Sci. Instrum.* **2012**, *83*, 113701.
(19) Sadewasser, S.; Carl, P.; Glatzel, T.; Lux-Steiner, M. -Ch. *Nanotechnology* **2004**, *15*, S14−S18.
(20) Ziegler, D.; Rychen, J.; Naujoks, N.; Stemmer, A. *Nanotechnology* **2007**, *18*, 225505.
(21) Ziegler, D.; Naujoks, N.; Stemmer, A. *Rev. Sci. Instrum.* **2008**, *79*, 063704.
(22) Tekiel, A.; Miyahara, Y.; Topple, J. M.; Grutter, P. *ACS Nano* **2013**, *7*, 4683−4690.
(23) Haynes, W. M. *CRC Handbook of Chemistry and Physics*, 93rd ed.; Taylor & Francis: Boca Raton, FL, 2012.
(24) Michaelson, H. B. *J. Appl. Phys.* **1977**, *48*, 4729−4733.
(25) Besocke, K.; Krahl-Urban, B.; Wagner, H. *Surf. Sci.* **1977**, *68*, 39−46.
(26) Jackson, J. D. *Classical Electrodynamics*, 2nd ed.; Wiley: New York, 1975.
(27) Magid, I.; Burstein, L.; Seitz, O.; Segev, L.; Kronik, L.; Rosenwaks, Y. *J. Phys. Chem. C* **2008**, *112*, 7145−7150.
(28) Hacker, C. A. *Solid-State Electron.* **2010**, *54*, 1657−1664.
(29) Yaffe, O.; Scheres, L.; Segev, L.; Biller, A.; Ron, I.; Salomon, E.; Giesbers, M.; Kahn, A.; Kronik, L.; Zuilhof, H.; Vilan, A.; Cahen, D. *J. Phys. Chem. C* **2010**, *114*, 10270−10279.
(30) Gomila, G.; Toset, J.; Fumagalli, L. *J. Appl. Phys.* **2008**, *104*, 024315.
(31) Yoo, M. J.; Fulton, T. A.; Hess, H. F.; Willett, R. L.; Dunkleberger, L. N.; Chichester, R. J.; Pfeiffer, L. N.; West, K. W. *Science* **1997**, *276*, 579−582.

dx.doi.org/10.1021/nl503782s | *Nano Lett.* 2015, 15, 51−55